Domain growth dynamics and local viscosity in stratifying foam films

Peter Heinig,* César Márquez Beltrán, and Dominique Langevin
Laboratoire de Physique des Solides, UMR 8502-Université Paris-Sud, Bat. 510, 91405 Orsay (France)
(Received 4 October 2005; revised manuscript received 31 January 2006; published 24 May 2006)

We present a quantitative theory and experiments for the expansion dynamics of domains in stratifying foam films. Foam films containing micelles, colloidal particles or polymer-surfactant complexes often form layered structures and thin in a stepwise fashion: circular domains of lower thickness are formed and expand following a $R(t) \propto t^{1/2}$ law. In the present paper the film is modeled by an incompressible three-dimensional fluid with incompressible surfaces. The film tension difference between the film and domains results in the formation of a rim at the domain boundary and a gradient in film thickness and pressure in the surrounding film. The material transport due to this gradient lets the domains grow. We present experiments utilizing the thin balance method to qualitatively confirm the thinning mechanism and to determine material parameters including local film viscosity of a film composed of 4400 ppm acrylamide/acrylamidomethylpropanesulfonate-copolymer and 0.06 mmol/l dodecyltrimethylammonium bromide solution. We found a film viscosity of about 60 times the bulk viscosity, consistent with previous measurement in the same system but using another method.

DOI: 10.1103/PhysRevE.73.051607 PACS number(s): 68.15.+e, 66.20.+d, 61.20.−p, 66.10.−x

I. INTRODUCTION

The rheological properties of confined fluids are of special interest for modern technology, for example, the development of microfluidic and nanofluidic devices, and subject of basic research within the recent years. In free standing foam films the liquid is confined on nanometer scale and films containing micelles [1,2], colloidal particles [3], or polyelectrolyte/surfactant mixtures [4,5] exhibit local ordering resulting in a stepwise thinning of the film. The phenomenon can be understood in terms of an oscillating disjoining pressure isotherm (sketch in Fig. 1) such that several metastable film thicknesses can coexist for one applied pressure. During the film thinning circular spots of a lower metastable thickness occur, expand and finally cover the whole film area. Then the process is repeated until the film breaks or a thin black film remains. Kralchevsky *et al.* [6] found that the time evolution of the domain radii follows a power law $R(t) \propto t^{1/2}$ or, in other words, a constant change rate of the domain area. In some systems at a critical domain radius satellite droplets are formed [7,8] which is attributed to a Rayleigh type instability of the rim. In the presence of satellite droplets the behavior of the domain growth dynamics changes $[R(t) \propto t]$ [8,9]; subject of the present paper is the $R(t) \propto t^{1/2}$ regime without satellite droplets.

Kralchevsky *et al.* [6] proposed a diffusive-osmotic mechanism in order to explain the experimentally observed $R(t) \propto t^{1/2}$ behavior. Within this model the domain formation is interpreted as a phase transition of low-thickness sites (vacancies) and high-thickness sites (spots), where the domains represent a vacancy-rich phase and the surrounding film a vacancy-poor phase. Due to a gradient in chemical potential at the periphery of the film vacancies are produced at a constant rate, they diffuse inside the film, and nucleate at the domain and make it grow. The diffusion of vacancies is assumed to be fast, such that the production rate of vacancies at the periphery governs the dynamics of domain growth and leads to a total domain phase fraction growing proportional in time.

The diffusive-osmotic mechanism gives a plain and elegant explanation for the observed power law. However, it does not yield quantitative predictions, such as the influence of material parameters on the domain expansion dynamics. Also, experiments presented in the present paper point toward a local mechanism rather than a domination of the film periphery. Márquez-Beltrán *et al.* [10] reported an experimental comparison of the growth rates as a function of film composition. It has been found that the growth rates strongly depend on the charge and concentration of the surfactant, indicating a strong variation of local viscosity or structural forces depending on film composition. For the identification of confinement effects on viscosity and structural forces a quantitative theory is necessary. In the next section a local-diffusive mechanism will be proposed.

II. THEORY

A. Hydrodynamic problem

Commonly thin liquid films are modeled within the lubrication approximation [11], i.e., with negligible inertia (creep-

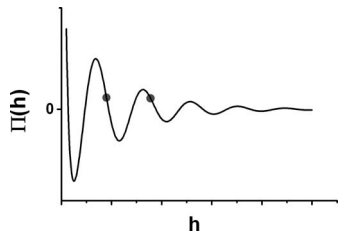

FIG. 1. Sketch of an oscillating disjoining pressure isotherm in arbitrary units (line). Films thicknesses with $\frac{\partial \Pi}{\partial h} > 0$ are unstable. For an applied pressure Π several metastable film thicknesses can coexist (gray dots).

*Electronic address: peter.heinig@ds.mpg.de

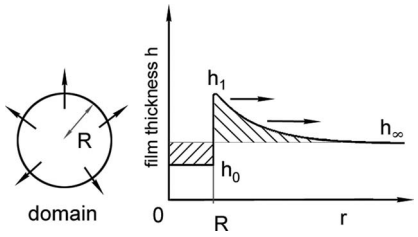

FIG. 2. Sketch of a growing domain of radius R. The film thickness equals h_0 inside the domain and h_∞ at infinity. The film tension difference between inside and outside (driving force) results in a rim with height h_1. Material is transported (marked by black arrows) from the inside of the domain into the surrounding film (hatched regions).

ing flow limit) and a small film thickness compared to the lateral extension of film. The assumption of an incompressible monolayer at the two surfaces leads in the case of film drainage to a no-slip (Poiseuille) boundary condition and is experimentally well confirmed. Also, experiments in thin liquid films [12] showed a low compressibility of the film surface, which is explained by the limited amount of surfactant available for transfer. However, experimentally observed phenomena such as surface waves [13,14] are commonly modelled by taking surfactant transfer from the surface to interior of the film into account. In the further treatment we assume that the film surface is incompressible.

Assume a circular domain of radius R embedded within a film of equilibrium thickness h_∞ (Fig. 2). The equilibrium thickness within the domain is $h_0 < h_\infty$, where $h_\infty - h_0$ corresponds to the thickness of one stratum in the stratified film. The film tension of the thinner film inside the domain is smaller than of the film outside the domain—the system is out of equilibrium favoring the thinner film and the film tension difference $\Delta\sigma$ acts as a driving force for enlarging the domain. In the present theory the domain growth dynamics is modeled by the dynamics of material transport in the film surrounding the domain. The geometry is axially symmetric and the film thickness is described by the profile $h(r,R)$, with $h(r,R)=h_0$ for $r<R$ and $\lim_{r\to\infty} h(r,R)=h_\infty$ at infinity. The driving force $\Delta\sigma$ is assumed to result in an increase of the film thickness at the rim $h(r=R,R)=h_1$, where h_1 is another material constant. Note that the exact shape of the rim is not known and its determination requires a more detailed model than the concept of disjoining pressure depending only on the thickness of the film. However, the shape of the rim close to the domain boundary has no effect if the material flow through the surroundings dominates the dynamics. The experimental observation of satellite droplets is an indication for the existence of the rim.

In the creeping flow limit the Navier-Stokes and the continuity equations lead to the following expression [11]:

$$\frac{\partial h}{\partial t} = \frac{h^3}{12\eta}\Delta P, \tag{1}$$

where Δ is the Laplace operator and P denotes the pressure in the film. Although the film viscosity η is expected to depend on the film thickness, as a first approximation η will be assumed constant. For $h \approx h_\infty$, with a linear approximation for the disjoining pressure

$$P = P_0 - \frac{\partial \Pi}{\partial h}(h - h_\infty), \tag{2}$$

with P_0 the surrounding air pressure, Eq. (1) can be written as

$$\frac{\partial h}{\partial t} = -\frac{h^3}{12\eta}\frac{\partial \Pi}{\partial h}\Delta h. \tag{3}$$

Since generally $(h_1 - h_\infty) \ll (h_\infty - h_0)$ Eq. (3) coincides with a 2D diffusion equation

$$\frac{\partial h}{\partial t} = D\Delta h, \tag{4}$$

with the diffusion constant

$$D = -\frac{h_\infty^3}{12\eta}\frac{\partial \Pi}{\partial h}. \tag{5}$$

Note that a similar relation is found for the spreading of flat droplets on a solid substrate [15]. Equation (5) relates the unknown viscosity to the disjoining pressure isotherm and diffusion constant, which can be determined as described below.

Rewriting Eq. (4) in polar coordinates yields

$$\frac{\partial h}{\partial t} = D\frac{1}{r}\frac{\partial}{\partial r}\left(r\frac{\partial h}{\partial r}\right). \tag{6}$$

This differential equation has to be solved for the profile $h[r,R(t),t]$, while the total volume of material is conserved

$$\pi R^2(h_\infty - h_0) = \int_R^\infty 2\pi r[h(r,R) - h_\infty]dr. \tag{7}$$

B. Stationary solution for the renormalized profile

Generally, different profiles evolve differently in time. We are especially interested in stationary profiles, i.e., profiles which keep their shape in time. Since R is not a constant it is useful to use the renormalized profile $h(r,R)=h(r/R)=h(x)$, where R plays the role of a scaling parameter. Note that using this ansatz equation (7) is invariant with respect to a scale transformation $R \to R'$.

The calculation is performed in Appendix A and one finds the profile

$$h = \frac{h_1 - h_\infty}{\mathrm{Ei}\left(-\frac{C}{4D}\right)}\mathrm{Ei}\left(-\frac{C}{4D}x^2\right) + h_\infty, \tag{8}$$

with a constant domain growth velocity $C=\frac{dR^2}{dt}$, and the exponential integral function Ei. Volume conservation yields a relation between C and D (see the Appendix):

$$\frac{h_\infty - h_0}{h_1 - h_\infty} + 1 = -\frac{4D}{C}\frac{e^{-C/4D}}{\mathrm{Ei}\left(-\frac{C}{4D}\right)}. \tag{9}$$

For the realistic case $(h_\infty - h_0) \gg (h_1 - h_\infty)$, Eq. (9) can be approximated by

$$\frac{h_\infty - h_0}{h_1 - h_\infty} \approx -\frac{4D}{C}\frac{1}{\gamma + \ln\frac{C}{4D}}, \tag{10}$$

with $\gamma = 0.577\cdots$ being the Euler constant, or by

$$\frac{C}{4D} \approx \frac{h_1 - h_\infty}{h_\infty - h_0}\frac{0.785}{\ln\frac{h_\infty - h_0}{h_1 - h_\infty}}. \tag{11}$$

C. Driving force and disjoining pressure isotherm

The disjoining pressure at the rim compensates the average pressure due to surface tension difference

$$\Pi(h_1) - \Pi(h_\infty) = -\frac{\int_{h_0}^{h_\infty}\Pi(h)dh}{\int_{h_0}^{h_\infty}dh} = \frac{\Delta\sigma}{h_\infty - h_0}, \tag{12}$$

where the expression

$$\Delta\sigma = -\int_{h_0}^{h_\infty}\Pi(h)dh \tag{13}$$

has been used. With a linear approximation of the disjoining pressure for small distortions this leads to

$$h_1 - h_\infty = \frac{-\Delta\sigma}{h_\infty - h_0}\Big/\frac{\partial\Pi}{\partial h}. \tag{14}$$

Note that in Eq. (14) the derivative of $\Pi(h)$ as well as its integral occurs. The disjoining pressure isotherm has therefore to be known very well in order to get reasonable predictions. Experimentally measured disjoining isotherms [16], as well as structural forces close to the surface of bulk solutions [17], can be well described by a damped oscillation, which is also predicted by semiempirical theories [18]. In the further treatment we will therefore assume a damped oscillating disjoining pressure isotherm which reduces the number of material parameters to a minimum. However, the assumption is a potential source of errors and it has to be dealt as a simplistic mathematical ansatz describing the observed behavior with as few as possible parameters.

Assume an oscillating disjoining pressure isotherm of the form

$$\Pi(h) = -A\sin\left(\frac{2\pi h}{\tilde{h}} + \phi_0\right)e^{-h/h^*}, \tag{15}$$

where A is the amplitude, $\tilde{h}$ is the period, and h^* is the decay length. If $\Pi(h)$ is sufficiently small the period coincides with the step width $\tilde{h} \approx h_\infty - h_0$ and the film thickness at equilibrium h_∞, respectively, h_0 is a linear function of the number of layers $h_\infty = \tilde{h}\left(n - \frac{\phi_0}{2\pi}\right)$, respectively, $h_0 = \tilde{h}\left(n - 1 - \frac{\phi_0}{2\pi}\right)$. The derivative of $\Pi(h)$ of equilibrium thicknesses therefore reads

$$\left.\frac{\partial\Pi}{\partial h}\right|_{h=\tilde{h}\left(n-\frac{\phi_0}{2\pi}\right)} = -A\frac{2\pi}{\tilde{h}}e^{-(n-\phi_0/2\pi)\tilde{h}/h^*}. \tag{16}$$

The surface tension difference between layer n and the domain with $n-1$ layers is obtained by solving the integral (13) with the disjoining pressure (15)

$$\Delta\sigma = -\frac{2\pi A\tilde{h}}{(\tilde{h}/h^*)^2 + (2\pi)^2}e^{-(n-\phi_0/2\pi)\tilde{h}/h^*}(1 - e^{\tilde{h}/h^*}). \tag{17}$$

Substituting this into Eq. (14) yields

$$h_1 - h_\infty = \frac{\tilde{h}}{(\tilde{h}/h^*)^2 + (2\pi)^2}(e^{\tilde{h}/h^*} - 1). \tag{18}$$

It is remarkable that $h_1 - h_\infty$ does not depend on the amplitude A and, for the assumed isotherm, also not on the layer number n. The theory can now be applied to experimental observations.

D. Remarks and qualitative predictions

The relations between expansion velocity C and diffusion constant D are only valid if the domain is "free" and far away from the meniscus of the film. The expression

$$l = R\sqrt{\frac{h_\infty - h_0}{h_1 - h_\infty}} \tag{19}$$

is a characteristic length and corresponds to the radius r at which deviations from the equilibrium film thickness can be neglected $(h \approx h_\infty)$. The presented theory applies only if the film is sufficient compressible [small $-\frac{\partial\Pi}{\partial h}$, large $(h_1 - h_\infty)$, small l]. Then each domain i is expected to grow independently from the others with a constant velocity

$$\frac{dR_i^2}{dt} = \text{const} \quad \text{for all } i. \tag{20}$$

The osmotic-diffusive mechanism proposed by Kralchevsky *et al.* [6] predicts a different qualitative behavior: Within the diffusive-osmotic model the domain expansion dynamics is governed by material transport through the film periphery and the domain formation is interpreted as a phase transition. A gradient in osmotic pressure at the film periphery results in a constant production rate of vacancies, which diffuse inside the film and nucleate at the domain. The diffusion is assumed to be fast such that the vacancy production at the periphery governs the dynamics of domain expansion and leads to a constant transport rate of material through the film periphery

$$\frac{dA}{dt} = \sum_i \pi\frac{dR_i^2}{dt} = \text{const}. \tag{21}$$

Here, only for a single domain the $R(t) \propto t^{1/2}$ behavior is expected. If new domains are formed the domain growth velocities of the individual domains is expected to decrease.

Finally, we want to mention a model proposed by de Gennes and Cazabat [19] in order to describe the dewetting of stratified polymer melts on solid substrates and potentially

interesting for the present subject. De Gennes and Cazabat model the stratification layers of the film by incompressible 2D liquids sliding on each other. It is assumed that dissipation is governed by friction between the layers. In Appendix B we show that, independent of the friction mechanism, the experimentally observed $R(t) \propto t^{1/2}$ regime cannot be explained within this model, which predicts an exponent of the power law of at least 2/3.

III. EXPERIMENTAL

The experiments were performed with a thin film balance using the porous plate technique [20–22], a porosity of 100 μm has been used. The film was observed by an optical microscope and the images were videotaped (25 frames per second), the film thickness was measured using the microinterferometric method of Scheludko [23]. We used a sample solution of 4400 ppm acrylamide/acrylamidomethylpropanesulfonate-copolymer (PAMPS) and 0.06 mmol/l dodecyltrimethylammonium bromide (DTAB). The polymer, with a number fraction of charged monomers of 50%, was provided by SNF Floerger and purified using an ultrafiltration unit with a 20 000 Da cutoff membrane. Also a sample of 1000 ppm blanose sodium carboxymethylcellulose 12M31P (CMC) and 0.01 mM cetyltrimethylammonium bromide (CTAB) was used. The CMC has been supplied by Aqualon Hercules (minimum purity of 99.5% related to dry matter: carboxyMC is known to be highly hydrated) and used without further purification. The substitution degree (average number of carboxymethyl groups per glucose unit) is 1.23. The surfactants have been purchased from Aldrich and recrystallized three times from acetone-ethanol solution (24:1) before usage. The surfactant concentration was chosen such as to avoid the presence of surfactant-polymer aggregates in the solution (surfactant concentration below the critical aggregation concentration). The polymer concentration is above C^*, the overlap concentration of chains, and the solution is semidilute; the polymer chains form a network of mesh size ξ, unaffected by the presence of surfactant. In this case, film stratification is associated to the network, and not to the presence of micelles. The elementary step of stratification $\tilde{h}$ was found equal to ξ in good approximation [24]. Although there are no polymer surfactant aggregates in bulk, the two species aggregate at the film surfaces, allowing the film to be stable (without polymer, the surfactant solutions are so dilute that the films are unstable). The mixed surfactant polymer surface layer is extremely thin, of the order of 2 nm, because the polymer adsorbs in a flat configuration [25].

A. Hydrodynamic mechanism and domain growth velocities

Figure 3 shows the square of the domain radius versus time in the $2 \rightarrow 1$ layer of PAMPS-DTAB. The domains are relatively small compared to the film size and separated (image), the rim is not visible. The domain growth velocity is roughly constant for all the domains while the total area change rate increases stepwise when new domains are formed. If the domain is close to the meniscus, as in a CTAB-CMC system shown in Fig. 4, the periphery influences the domain growth dynamics and the growth rate increases with the size of the domain. This behavior cannot be explained by the diffusive-osmotic model where the production rate of vacancies at the periphery should be unaffected by structural properties of the interior.

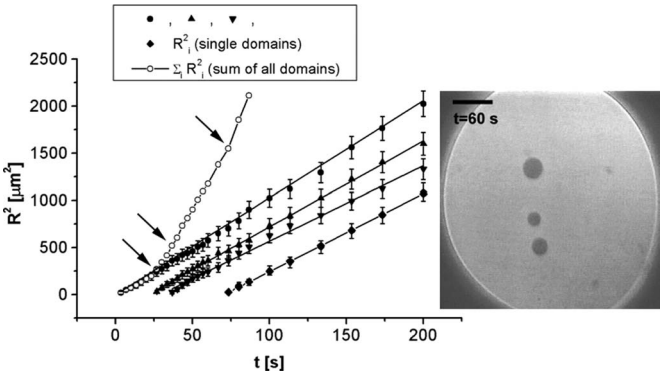

FIG. 3. Domain growth in the $2 \rightarrow 1$ layer of a film composed of PAMPS-DTAB solution. The domains are small compared to the film radius and relatively isolated (image right). The graph shows the square of the domain radii versus time (solids) and repective linear fits (lines). Also shown is the total change in domain area within the film (open circle) with arrows marking the times when new domains appear. The bar represents 100 μm.

The measured values of domain growth velocities in PAMPS-DTAB are $\left(\frac{dR^2}{dt}\right)_{2\rightarrow 1}=(8.9\pm 0.5)\ \mu\text{m}^2/\text{s}$ in the $2 \rightarrow 1$ layer and $\left(\frac{dR^2}{dt}\right)_{3\rightarrow 2}=(10.26\pm 1.0)\ \mu\text{m}^2/\text{s}$ in the $2 \rightarrow 3$ layer (in CMC-CTAB the domain growth velocity increases from 35 to 90 $\mu\text{m}^2/\text{s}$). Stratification is observed also for thicker films. However, since domains are formed very close to each other and coalesce often it was not possible to measure the domain growth velocity. From film observation one can only state that it is slower than in the thinner films. The period $\tilde{h}$ is found to be $\approx$20 nm.

B. Determination of the diffusion constant D and decay length h^*

The domain growth velocities at two different film thicknesses determine the unknown decay length h^*. Since the

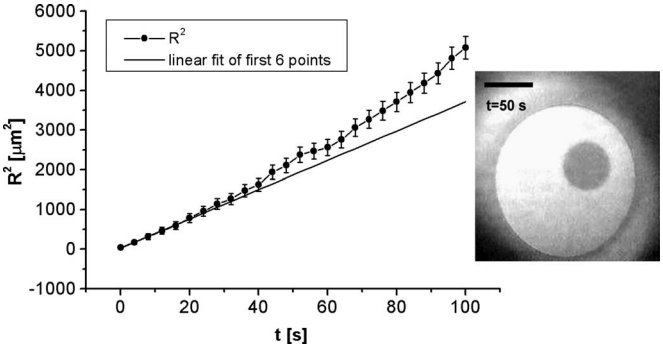

FIG. 4. Domain growth in the $2 \rightarrow 1$ layer a of film composed of CTAB-CMC solution. The graph shows the square of the domain radius versus time and a remarkable increase of the growth rate in time. In this example the growth is governed by local diffusion as well as the film periphery.

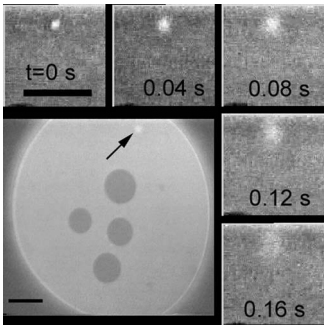

FIG. 5. Image of the $2 \rightarrow 1$ layer composed of PAMPS-DTAB solution. The bright spot (arrow) broadens in time and finally disappears as shown in the images at the edge (here the contrast has been increased). The bars correspond to 100 μm.

left-hand-side of Eq. (9) is a constant (18) and the right-hand side depends only on D/C, for different layers also the ratio D/C has to be equal. Namely, for the two measured domain growth velocities

$$\frac{D_{2\rightarrow 1}}{C_{2\rightarrow 1}} = \frac{D_{3\rightarrow 2}}{C_{3\rightarrow 2}}. \tag{22}$$

Substituting Eqs. (5) and (16) into this equation yields

$$\frac{2^3}{C_{2\rightarrow 1}} e^{-2\tilde{h}/h^*} = \frac{3^3}{C_{3\rightarrow 2}} e^{-3\tilde{h}/h^*} \tag{23}$$

and finally

$$\frac{\tilde{h}}{h^*} = -\ln\left(\frac{8}{27}\frac{C_{3\rightarrow 2}}{C_{2\rightarrow 1}}\right) \approx 1.07. \tag{24}$$

Plugging this into Eq. (18) yields

$$h_1 - h_\infty \approx 0.047\tilde{h}. \tag{25}$$

This means that at the rim of the domain the film thickness increases by 5% (with respect to thickness of one layer $\tilde{h}$), which is a quite reasonable result. Plugging this into Eq. (9) yields the diffusion constants $D_{2\rightarrow 1} \approx 184$ μm^2/s and $D_{3\rightarrow 2} \approx 212$ μm^2/s.

With the amplitude A of the disjoining pressure isotherm the viscosity can easily be determined using Eq. (5). Before the amplitude (and the contact angle with the meniscus) is obtained by evaluation of the film size we want to check the consistency of the obtained results by a direct measurement of the diffusion constant.

C. Direct measurement of the diffusion constant

Figure 5 shows an event where a bright spot, a micron-sized droplet from the surrounding air, spreads into the film.

The width of the spot, i.e., the mean square deviation σ^2, can be directly determined by image analysis:

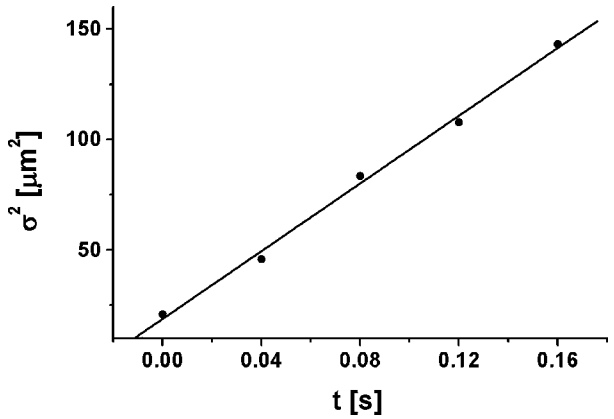

FIG. 6. Mean square deviation (26) of the event in Fig. 5 in dependence of time (symbols) and a linear fit (line). The slope corresponds to four times the diffusion constant D.

$$\sigma^2 = \frac{\int [h(r) - h_\infty] r^2 dr}{\int [h(r) - h_\infty] dr}, \tag{26}$$

where r denotes the distance from the center of the spot and $h(r)$ is obtained by averaging $h(r, \phi)$ along a circle. The result is shown in Fig. 6.

The time dependence is linear with a slope of (766 ± 28) μm^2. With the equation

$$\sigma(t)^2 = 4Dt \tag{27}$$

one finds for the diffusion constant $D_{2\rightarrow 1} = (192 \pm 7)$ μm^2/s. The agreement with the diffusion constant determined before (184 μm^2/s) is excellent.

D. Contact angle θ and amplitude A by film size measurement

The contact angle θ between the film and the meniscus is determined by the force equilibrium

$$\cos\theta = \frac{\sigma}{2\sigma_0}, \tag{28}$$

where σ_0 is the bulk surface tension; it equals 55.6 mN/m for the investigated PAMPS-DTAB solution. The film tension can be written as

$$\sigma = \sigma_0 + \frac{1}{2}\int_h^\infty \Pi(\xi) d\xi \tag{29}$$

and one finds

$$\cos\theta = -\frac{\pi A \tilde{h}}{\sigma_0[(\tilde{h}/h^*)^2 + (2\pi)^2]} e^{-(n-\phi_0/2\pi)\tilde{h}/h^*} + 1. \tag{30}$$

So, the contact angle strongly depends on the amplitude A and a measurement of θ allows its determination. The common way for measurement of the contact angle described in literature [26] is by measuring the distance between Newton fringes at the film-meniscus boundary. However, Newton

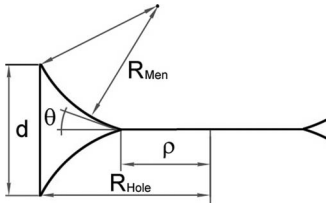

FIG. 7. Sketch of the film formed in the Scheludko cell with a hole radius R_{hole} and a hole thickness d. The radius of the meniscus R_{men} is determined by the applied pressure ΔP and the surface tension σ_0 described by the Young-Laplace equation. Measurement of the film radius ρ reveals information about the unknown contact angle θ.

fringes are resolvable only if the curvature radius of the meniscus and contact angle are sufficiently small. In the experiments described here Newton fringes are not resolvable and another method has to be applied.

Another possibility is to measure the radius of the film ρ in dependence of the pressure (sketch in Fig. 7). The curvature radius R_{men} of the meniscus is determined by the Young-Laplace equation

$$R_{\text{men}} = \frac{2\sigma_0}{\Delta P}, \tag{31}$$

where ΔP is the difference between air pressure and the pressure of the bulk solution in the Scheludko cell. One finds for the contact angle

$$\cos\theta = \frac{d}{4R_{\text{men}}} + \frac{R_{\text{hole}} - \rho}{2R_{\text{men}}}\sqrt{\frac{4R_{\text{men}}^2 - (R_{\text{hole}} - \rho)^2 - d^2/4}{(R_{\text{hole}} - \rho)^2 + d^2/4}}, \tag{32}$$

where R_{hole} is the radius of the hole in the Scheludko cell where the film is formed and d is its thickness.

Since we are interested only in A, rather than using Eq. (32) direct fitting of the measured $\rho(P_0)$ curve yields results less vulnerable to noise. For the film radius one finds the relation

$$(R_{\text{hole}} - \rho)^2 = -\frac{p}{2} \pm \sqrt{\frac{p^2}{4} - q}, \tag{33}$$

with

$$p = 4R_{\text{men}}^2\left(\cos\theta - \frac{d}{4R_{\text{men}}}\right)^2 + \frac{d^2}{4} - 4R_{\text{men}}^2, \tag{34}$$

$$q = 4R_{\text{men}}^2\left(\cos\theta - \frac{d}{4R_{\text{men}}}\right)^2\frac{d^2}{4}. \tag{35}$$

Here, the $-$ gives the meaningful solution.

Figure 8 shows the film radius ρ in dependence of the pressure P_0. The fits were obtained using Eq. (33), and substituting Eqs. (34), (35), and (30), and fitting the amplitude A. With $R_{\text{hole}}=0.69$ mm, $d=0.9$ mm one finds $A=(6\pm1)\times10^5$ Pa, which is compatible to the disjoining pressure isotherms measured by Asnacios *et al.* [24]. Note that the direct measurement of the disjoining pressure isotherms yields only

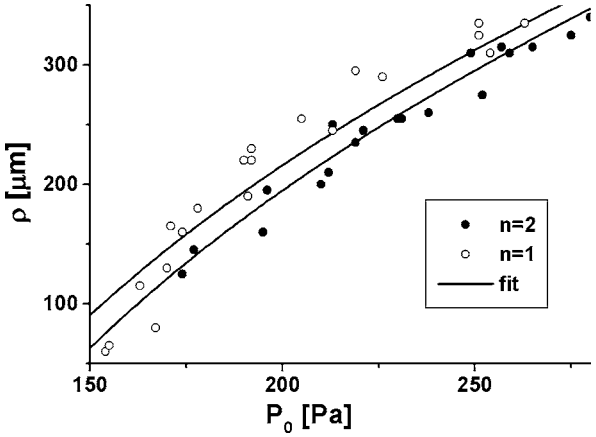

FIG. 8. Film radius ρ in dependence of pressure P_0 for PAMPS-DTAB film with one and two layers (symbols). The film tension of the thinner film is smaller leading to a larger contact angle and film radius. The lines were obtained by fitting the amplitude A to the data of both film thicknesses using Eq. (33).

information about the stable branches and a lower limit for the amplitude. The measured amplitude coincides to the contact angles $\theta_{n=1}=6.2^\circ$ and $\theta_{n=2}=3.7^\circ$, which are remarkably larger than the contact angles measurable using the Newton-fringe method [6].

Now, the local film viscosity can be calculated from the diffusion constant (5) and the derivative of the disjoining pressure (16). One finds $\eta\approx0.67$ Pas (viscosity in bulk ≈10.4 mPa s), which is consistent with former measurements in the same system finding a lower limit of 0.33 Pas [27]. The increase compared to bulk viscosity (10.4 mPa s) can be explained by strong interactions between the oppositely charged polyelectrolyte and surfactant [24].

IV. RESULTS AND DISCUSSION

We proposed a mechanism of domain growth, were material from the interior of the domain is transported by a diffusive process to the surrounding film. The comparison of qualitative predictions with other models (diffusive-osmotic model, and incompressible-layer model) and experiments in films composed of PAMPS-DTAB and CTAB-CMC yield the following results.

For isolated bubbles the local-diffusive model correctly predicts $R(t)\propto t^{1/2}$ (so does the diffusive-osmotic model but not the incompressible layer model).

For nonisolated (large) bubbles the growth velocity increases in time, as predicted by the local-diffusive model and the incompressible-layer model (Fig. 4). Within the diffusive-osmotic model it is not possible to explain this increase.

Experimentally it was found that, if many isolated bubbles are present in the same film, they grow independently of the number of bubbles with a constant growth velocity (Fig. 3). This clearly indicates a local mechanism with no influence of the meniscus (as in the diffusive-osmotic model) or the distance of the bubble to the film periphery.

The dynamics of domain growth can be described completely if the disjoining pressure of the investigated system is

known. However, since the accuracy of the experimental disjoining pressure isotherm is very limited, assumptions have to be made, and the disjoining pressure isotherm remains as the largest uncertainty of the model. We assumed a damped oscillating disjoining pressure isotherm reducing the parameters to amplitude A, period $\tilde{h}$, and damping length h^*. This assumption has to be dealt as a simplistic ansatz explaining the stratification phenomenon with as few as possible parameters. The isotherm parameters were measured for PAMPS-DTAB in the following way: the period $\tilde{h} \approx 20$ nm has been determined by film thickness measurement using the microinterferometric method. Note that the mixed polymer-surfactant layer at the film surfaces is much thinner, so that we did not need to take it into account (all the layers were assumed to have the same thickness). The damping length h^* can be calculated if the domain growth velocities of at least two layers of the film are known, in the investigated system $h^* \approx 18.7$ nm has been found. The amplitude $A \approx 6.2 \times 10^5$ Pa has been determined by contact angle measurements, were the contact angle has been determined by film size measurement.

Using this parameters the diffusion constant and local viscosity have been determined from the domain growth velocity. Comparing the so found diffusion constant to the directly measured value yields a good agreement (184 $\mu m^2/s$ from domain growth and 192 $\mu m^2/s$ from direct measurement) and confirms the validity of the applied theory. For the film viscosity a value of $\eta \approx 0.67$ Pa has been found, which is consistent with the previously measured lower limit of 0.3 Pa in the same system [27]. In Ref. [27], the relaxation dynamics of deformed domain shapes has been analyzed, and in particular no assumptions about the disjoining pressure isotherm had to be made.

Both approaches to local viscosity yield a consistent picture and can be applied in future in order to identify confinement effects and their dependence on film compositions. Which approach will be used can be chosen depending on the kind and quality of the observed events. In order to apply the presented method stratification has to observed for at least two layers and the formed domains must not be too close. This behavior is frequently observed and we believe that the presented method can potentially be applied to films of various compositions.

ACKNOWLEDGMENTS

We like to thank Nirmesh Jain for purifying the chemicals. P.H. would like to thank the franco-german network "Complex Fluids from 3D to 2D" for providing financial support.

APPENDIX A: FILM PROFILE FOR LOCAL DIFFUSIVE MECHANISM

The profile $h(r,R)=h(r/R)=h(x)$ is assumed to be stationary in the sense, that the time evolution always transforms the profile to itself on another scale $h(x) \rightarrow h(x)$, while $R(t) \rightarrow R(t+\delta t)$:

$$\left[h\left(\frac{r}{R}\right) + \frac{\partial h}{\partial t}\delta t \right]_{r,R} = h\left(\frac{r}{R+\delta R}\right). \tag{A1}$$

For small δR and $\frac{\delta R}{\delta t} \rightarrow \frac{dR}{dt}$ one finds

$$0 = \frac{\partial h}{\partial \frac{r}{R}} \frac{r}{R^2} \frac{dR}{dt} + \frac{\partial h}{\partial t}. \tag{A2}$$

Using Eq. (6) and rewriting Eq. (A2), using $x=r/R$, yields

$$0 = \frac{r}{R^2}\frac{\partial h}{\partial x}\frac{dR}{dt} + D\left(\frac{1}{rR}\frac{\partial h}{\partial x} + \frac{1}{R^2}\frac{\partial^2 h}{\partial x^2}\right) \tag{A3}$$

and finally

$$0 = h' x R \frac{\mathrm{d}R}{\mathrm{d}t} + D\left(\frac{h'}{x} + h''\right). \tag{A4}$$

Since $h(x)$ is not explicitly time dependent the domain growth velocity $\frac{\mathrm{d}R^2}{\mathrm{d}t} = C$ is a constant. The integration can be performed by separation of the variables

$$-\frac{dh'}{h'} = \left(\frac{Cx}{2D} + \frac{1}{x}\right)dx, \tag{A5}$$

and one finds

$$h' = c_1 \frac{\mathrm{e}^{-(C/4D)x^2}}{x}, \tag{A6}$$

where c_1 is the integration constant. Second integration leads to

$$h = \frac{c_1}{2}\mathrm{Ei}\left(-\frac{C}{4D}x^2\right) + c_2, \tag{A7}$$

with the integration constant c_2 and $\mathrm{Ei}(x) = \int_{-\infty}^{x} \frac{e^t}{t} dt$ being the exponential integral function.

The integration constants c_1 and c_2 are determined by the boundary conditions $h(1)=h_1$ and $\lim_{x\rightarrow\infty} h(x)=h_\infty$ and one gets

$$h = \frac{h_1 - h_\infty}{\mathrm{Ei}\left(-\frac{C}{4D}\right)}\mathrm{Ei}\left(-\frac{C}{4D}x^2\right) + h_\infty. \tag{A8}$$

The constant C is determined by the volume conservation equation (7). With the substitution $\rho=(r/R)^2$ one finds

$$\frac{h_\infty - h_0}{h_1 - h_\infty}\mathrm{Ei}\left(-\frac{C}{4D}\right) = \int_1^\infty \mathrm{Ei}\left(-\frac{C}{4D}\rho\right)d\rho \tag{A9}$$

$$= -\mathrm{Ei}\left(-\frac{C}{4D}\right) - \frac{4D}{C}e^{-C/4D} \tag{A10}$$

and finally

$$\frac{h_\infty - h_0}{h_1 - h_\infty} + 1 = -\frac{4D}{C}\frac{e^{-C/4D}}{\mathrm{Ei}\left(-\frac{C}{4D}\right)}. \tag{A11}$$

APPENDIX B: FRICTIONAL FORCE OF THE INCOMPRESSIBLE-LAYER MODEL

Consider a film composed of an incompressible layer sliding on a non moving substrate. The dynamics shall be dominated by friction between layer and substrate and the frictional force density per unit area f shall depend on the local velocity v in the following way:

$$f = \xi v^{\mu}, \tag{B1}$$

where ξ is the friction coefficient and the exponent μ describes the nature of the friction. In the macroscopic regime for slow motion the frictional force does not depend on the velocity, i.e., $\mu=0$ (Couloumb friction). On nanoscale other regimes are possible, so, for example, Stokes friction with $\mu=1$ as proposed by Prandtl [28].

Let the outflow at the rim of the domain equal $C=\frac{dR^2}{dt}$ then the continuity equation yields for all distances r from the center of the domain

$$v(r) = \frac{C}{2r}. \tag{B2}$$

The total frictional force is obtained by integration over the film area

$$F_{\text{fric}} = \int_R^{\rho} 2\pi r \xi v^{\mu} dr = \int_R^{\rho} 2\pi \xi (C/2)^{\mu} r^{1-\mu} dr, \tag{B3}$$

with the film radius ρ. For an infinite film this frictional force is finite only if $\mu>2$. The surface tension difference $\Delta\sigma$ results in a driving force proportional to R

$$F_{\text{fric}} = F_{\text{drive}} = \Delta\sigma R, \tag{B4}$$

and for $\mu \neq 2$ one finds

$$\frac{C}{2} = \frac{RdR}{dt} = \left(\frac{(2-\mu)\Delta\sigma R}{2\pi\xi(\rho^{2-\mu} - R^{2-\mu})} \right)^{1/\mu} \tag{B5}$$

and

$$\frac{dR}{dt} = \left(\frac{(2-\mu)\Delta\sigma R^{1-\mu}}{2\pi\xi(\rho^{2-\mu} - R^{2-\mu})} \right)^{1/\mu}. \tag{B6}$$

For $R \to \rho$ the domain growth velocity diverges and no power law holds. For $0<\mu<2$ (physical relevant case) and $\rho \gg R$ the denominator in Eq. (B6) is approximately constant. One finds

$$\frac{dR}{dt} \propto R^{-1+1/\mu} \tag{B7}$$

and after integration

$$R(t) \propto t^{1/(2-1/\mu)}. \tag{B8}$$

The exponent $\frac{1}{2-1/\mu}$ is for $\mu<2$ always larger than $2/3$ and cannot explain the experimentally observed $R(t) \propto t^{1/2}$. For example, for Stokes friction it equals one and the domain radius grows linear in time.

For $\mu=2$ it can be shown that the exponent equals $2/3$, and, finally, for $\mu>2$ the denominator in Eq. (B6) can be approximated by $-R^{2-\mu}$ and one finds

$$R(t) \propto t^{1/(1+1/\mu)}. \tag{B9}$$

Also for $\mu \geqslant 2$ the exponent is at least $2/3$ and the experimental behavior $R(t) \propto t^{1/2}$ cannot be explained.

[1] E. S. Johnnott, Philos. Mag. **70**, 1339 (1906).
[2] R. E. Perrin, Ann. Phys. **10**, 160 (1918).
[3] D. T. Wasan, A. D. Nikolov, P. A. Kralchevski, and I. B. Ivanov, Colloids Surf. **67**, 139 (1992).
[4] V. Bergeron and C. J. Radke, Langmuir **8**, 3020 (1992).
[5] V. Bergeron, D. Langevin, and A. Asnacios, Langmuir **12**, 1550 (1996).
[6] P. A. Kralchevsky, A. D. Nikolov, D. T. Wasan, and I. B. Ivanov, Langmuir **6**, 1180 (1990).
[7] V. Bergeron, A. I. Jiménez-Laguna, and C. J. Radke, Langmuir **8**, 3027 (1992).
[8] A. A. Sonin and D. Langevin, Europhys. Lett. **22**, 271 (1993).
[9] C. M. Beltrán and D. Langevin, Phys. Rev. Lett. **94**, 217803 (2005).
[10] C. Márquez-Beltrán, S. Guillot, and D. Langevin, Macromolecules **36**, 8506 (2003).
[11] J. E. Coons, P. J. Halley, S. A. McGlashan, and T. Tran-Congc, Adv. Colloid Interface Sci. **105**, 3 (2003).
[12] A. A. Sonin, A. Bonfillon, and D. Langevin, J. Colloid Interface Sci. **162**, 323 (1994).
[13] A. Vrij, Discuss. Faraday Soc. **42**, 23 (1966).
[14] R. Tsekov, H. J. Schulze, B. Radoev, and P. Letocart, Colloids Surf., A **142**(2-3), 287–294 (1998).
[15] J. F. Joanny and P.-G. de Gennes, J. Phys. (France) **47**, 121 (1986).
[16] C. Stubenrauch and R. von Klitzing, J. Phys.: Condens. Matter **15**, R1197 (2003).
[17] D. Qu, D. Baigl, C. E. Williams, H. Möhwald, and A. Fery, Macromolecules **36**, 6878 (2003).
[18] D. N. Petsev, N. D. Denkov, and P. A. Kralchevsky, J. Dispersion Sci. Technol. **18**, 647–659 (1997).
[19] P.-G. de Gennes and A.-M. Cazabat, C. R. Acad. Sci. Paris **310**, 1601 (1990).
[20] K. J. Mysels and M. N. Jones, Discuss. Faraday Soc. **42**, 42 (1966).
[21] D. Exerowa, T. Kolarov, and Khr. Khristov, Colloids Surf. **22**, 171 (1987).
[22] D. Exerowa and A. Scheludko, C. R. Acad. Bulg. Sci. **24**, 47 (1971).
[23] A. Scheludko and D. Platikanov, Kolloidn. Zh. **175**, 150 (1961).
[24] A. Asnacios, A. Espert, A. Colin, and D. Langevin, Phys. Rev. Lett. **78**, 4974 (1997).
[25] C. Stubenrauch, P. A. Albouy, R. von Klitzing, and D. Langevin, Langmuir **16**, 3206 (2000).
[26] A. Nikolov and D. T. Wasan, J. Colloid Interface Sci. **133**, 1 (1989).
[27] P. Heinig and D. Langevin, Eur. Phys. J. E **18**, 483 (2005).
[28] L. Prandtl, Z. Angew. Math. Mech. **8**, 85 (1928).